Journal of Molecular and Cellular Cardiology 157 (2021) 104–112

Contents lists available at ScienceDirect

Journal of Molecular and Cellular Cardiology

journal homepage: www.elsevier.com/locate/yjmcc

Dual role of miR-1 in the development and function of sinoatrial cells

P. Benzoni, L. Nava [1], F. Giannetti, G. Guerini, A. Gualdoni, C. Bazzini, R. Milanesi [2], A. Bucchi, M. Baruscotti, A. Barbuti [*]

The Cell Physiology MiLAb; Department of Biosciences, Università degli Studi di Milano, Milan, Italy

ARTICLE INFO

Keywords:
microRNA
miR-1
Sinus node
Embryonic stem cells
I_f current
HCN4

ABSTRACT

miR-1, the most abundant miRNA in the heart, modulates expression of several transcription factors and ion channels. Conditions affecting the heart rate, such as endurance training and cardiac diseases, show a concomitant miR-1 up- or down-regulation. Here, we investigated the role of miR-1 overexpression in the development and function of sinoatrial (SAN) cells using murine embryonic stem cells (mESC).

We generated mESCs either overexpressing miR-1 and EGFP (miR1OE) or EGFP only (EM). SAN-like cells were selected from differentiating mESC using the CD166 marker. Gene expression and electrophysiological analysis were carried out on both early mES-derived cardiac progenitors and SAN-like cells and on beating neonatal rat ventricular cardiomyocytes (NRVC) over-expressing miR-1.

miR1OE cells increased significantly the proportion of $CD166^+$ SAN precursors compared to EM cells (23% *vs* 12%) and the levels of the transcription factors TBX5 and TBX18, both involved in SAN development. miR1OE SAN-like cells were bradycardic (1,3 *vs* 2 Hz) compared to EM cells. In agreement with data on native SAN cells, EM SAN-like cardiomyocytes show two populations of cells expressing either slow- or fast-activating I_f currents; miR1OE SAN-like cells instead have only fast-activating I_f with a significantly reduced conductance. Western Blot and immunofluorescence analysis showed a reduced HCN4 signal in miR-1OE *vs* EM CD166+ precursors. Together these data point out to a specific down-regulation of the slow-activating HCN4 subunit by miR-1. Importantly, the rate and I_f alterations were independent of the developmental effects of miR-1, being similar in NRVC transiently overexpressing miR-1.

In conclusion, we demonstrated a dual role of miR-1, during development it controls the proper development of sinoatrial-precursor, while in mature SAN-like cells it modulates the HCN4 pacemaker channel translation and thus the beating rate.

1. Introduction

Heart development is a complex process that requires a precise temporal and spatial control of expression levels of many genes. This regulation involves microRNAs for modulating protein expression. Among the many miRNAs expressed during heart development, miR-1 is the most abundant in human and mouse heart [1]. miR-1 starts to be expressed in the mouse around E8.5 of development and its expression strongly increases after birth [2]. miR-1 derives from two transcripts (miR-1-1 and miR-1-2) with identical sequences, whose expression was reported both during cardiogenesis, in a chamber specific manner [3], and during mouse embryonic stem cell (mESC) differentiation, promoting mesoderm and cardiac formation [2]. Deletion of either miR-1-1 or miR-1-2 results in an analogue phenotype in mice: incompletely penetrant lethality, cardiomyocytes proliferative defects, and electrophysiological abnormalities; while the double knock-out is lethal before *E11.5* [4]. On the other hand, over-expression of miR-1 during heart development results in defective ventricular myocytes proliferation and causes hypoplasia of the cardiac ventricular conduction system [5,6]. So far, nothing is known regarding the specific effect of miR-1 on the development of sinoatrial (SAN) cardiomyocytes.

In the adult heart, miR-1 epigenetically modulates the expression of ion channels, connexins and regulatory proteins [7]. This regulation has an important role in the cardiac remodeling due to both pathological conditions, such as arrhythmic diseases (e.g. atrial fibrillation) [8], and physiological conditions, such as cardiac hypertrophy and bradycardia

* Corresponding author: Department of Biosciences, The Cell Physiology MiLAb, Università degli Studi di Milano, via Celoria 26, Milano 20133, Italy.
E-mail address: andrea.barbuti@unimi.it (A. Barbuti).
[1] Current address: Neuromodulation of Cortical and Subcortical Circuits Laboratory, Istituto Italiano di Tecnologia, Genova, Italy.
[2] Current address: Dipartimento di Medicina Veterinaria, Università degli Studi di Milano, Via dell'Università 6, 26900 Lodi, Italy.

https://doi.org/10.1016/j.yjmcc.2021.05.001
Received 7 September 2020; Received in revised form 27 April 2021; Accepted 3 May 2021
Available online 6 May 2021

following endurance training [9–11].

Here, we applied our previously published model of SAN-like cells derived from mESC [12], to specifically investigate and dissect the role of miR-1 in the development and function of the cardiac pacemaker.

2. Material and methods

2.1. mESC engineering and maintenance

Mouse ESCs (D3 line, ATCC-CRL11632) were grown and differentiated as embryoid bodies (EBs) as previously described [13].

To obtain mESC overexpressing miR-1 (miR1OE), downregulating miR-1 (ANTI-miR1) and the empty control line (EM), 2×10^6 cells were electroporated with 10 μg of linearized pEZX-MR04 plasmid or pEZX-AM02 plasmid (GeneCopoeia™) or empty vector (CmiR0001-MR04-GeneCopoeia™) using the A024 program of the Nucleofactor® II (Amaxa Byosystems) and the mESC Nucleofector kit (Lonza). Cells were then kept in stringent selection with 1 μg/mL puromycin for 2 weeks. The effect of puromycin selection was checked on non-electroporated mESC, which all died after 24–48 h in puromycin. After selection, single mESC colonies transfected with siRNA silencing miR-1 were manually picked using mCherry to clone only cells where the plasmid was properly integrated, while single mESC colonies transfected with miR-1 were sorted using the FACSAriaII flow-cytometer (BD Biosciences) by eGFP expression. This eGFP-based sorting procedure was repeated every 60–90 days on both EM and miR1OE mESC.

2.2. San-like CD166+ cell isolation and maintenance

EBs were detached from the plate at d8 of differentiation and dissociated to single cells for CD166-staining, as previously described [12]. Briefly, cells were incubated with the PE-conjugated rat anti-mouse CD166 antibody (eBioscience) or the corresponding isotype (PE-rat IgG) for 30 min at 4 °C under constant shaking. At the end of the incubation cells were washed and resuspended in PBS with the addition of 10% FBS, 1 mM $CaCl_2$ and 5 mmol/L EDTA. $CD166^+$cells were analyzed and sorted by FACSAriaII. $CD166^+$ cells were put to re-aggregate by gravity for 24 h in low-adhesion culture dishes in differentiating medium and subsequently plated at high density (5×10^4 cells/mm^2) to allow the formation of a compact layer, which was kept in culture for one week in differentiating medium supplemented with 2,5 μM ARA-C (Sigma-Aldrich). Molecular and electrophysiological analyses have been performed on the layers or on single cells following dissociation.

2.3. Proliferation analysis

EBs were collected from the plate at d6 of differentiation and dissociated to single cells using TryplE (Thermo-Fisher). Single cells suspension was fixed in cold ethanol at 70% for 1 h at −20 °C. Cells were incubated with the APC-conjugated anti-mouse Ki-67 antibody (Biolegend) or the corresponding isotype (APC-rat IgG) for 30 min at room temperature under constant shaking. At the end of the incubation cells were washed and resuspended in PBS with the addition of 10% FBS, 1 mM $CaCl_2$ and 5 mmol/L EDTA. Ki-67+ cells were analyzed by FACSAriaII.

2.4. Molecular analysis

Total mRNA was isolated using TRIzol (Thermo Fisher). Maxima First Strand cDNA synthesis kit (Thermo Fisher) was used to synthesize cDNA, while miRNAs were selected using miScript II RT Kit (Quiagen) following the manufacturer's instructions.

qRT-PCRs were performed in technical duplicate or triplicate using 10 ng cDNA with Maxima SYBR Green qPCR Master Mix (Thermo Fisher), or 2.5 ng miRNAs with miScript SYBR Green PCR Kit (Quiagen) in iCycler Bioer System (BIOER). Expression data were analyzed using 2^(-ΔCT) method relative to expression level of GAPDH as housekeeping gene or miR-16 as miRNA reference. Primers used are given below. qRT-PCR analysis was performed on differentiating cultures of at least 4 independent experiments.

OCT4 F:CTCCTTCTGCAGGGCTT R:GTTGGAGAAGGTGGAAAC

REX1 F:GGGCACTGATCCGCAAAC R:CAGCAGCTCCTGCACAC AGA

BRACHYURY-T F:GAAGAGCCTGCAGTACCGAG R:ACATCCTCC TGCCGTTCTTG

NODAL F:TACATCCAGAGCGTGCTGAAAC R:ACCCACACTCCTC CACAATC

GATA-4 F:GGAAGACACCCCAATCTCG R:CATGGCCCCACAATT GAC

NKX2.5 F:TTAGGAGAAGGGCGATGACT R:AGGTCCGAGACACC AGGCTA

SHOX2 F:GAAAGGACAAGGGCGTCA R:AACGTAGGTGCTTTAA GGATGC

TBX3 F:AGGAGCGTGTCTGTCAGGTT R: GCCATTACCTCCCCAA TTTT

TBX5 F:GGATGTCCTGGATGCAAAGT R:GGTTGGAGGTGACTTT GTGC

TBX18 F:TGATGGCCTCCAGAATGC R:CCGAGACTCTGGGAGG AAC

ISL1 F: CATCGAGTGTTTCCGCTGTGTAG R: GTGGTCTTCTCC GGCTGCTTGTGG

HCN1 F:CTCAGTCTCTTGCGGTTATTACG R:TGGCGAGGTCATA GGTCAT

HCN2 F:CCGCTGTTTGCCAATGC R:AGGCTGGAAGACCTCAAAT TTG

HCN4 F:GTCGGGTGTCAGGCGGGA R:GTGGGGGCCACCTGC TAT

CACNA1D F: GTTGTAAGTGCGGTAGAAAGCA R: CTGGTGCCTC TTGCATAGTTT

GJA1 F: GAACACGGCAAGGTGAAGAT R: GAGCGAGAGACACC AAGGAC

KCND2 F: TGGGCTACTGAGCAACCAG R: TGGATCCAGATTT GCTTATGAA

GAPDH F:TGTAGACCATGTAGTTGAGGTCA R:AGGTCGGTGTG AACGGATTTG

mmu -miR-1a-1-3p TGGAATGTAAAGAAGTATGTAT

mmu-miR-16-5P TAGCAGCACGTAAATTATTGGCG

2.5. Immunofluorescence and western blot analysis

MiR1OE and EM $CD166^+$ cells sorted by FACSAriaII at d8 of differentiation were solubilized in RIPA buffer. Western blot analyses were carried out loading 30 μg of whole cell protein extracts, separated by SDS-PAGE and transferred onto PVDF membranes. Antibodies used were anti-HCN1, anti HCN4 and anti-TNNT (1:1000; all from Thermo Fisher), and appropriate secondary antibodies HRP (Jackson ImmunoResearch, 1:10000). For chemiluminescent acquisition Chemidoc system (Bio-RAD) was used after membranes incubation with SuperSignal™ West Pico PLUS Chemiluminescent Substrate (Thermo Fisher).

SAN-like monolayers at d14 were fixed in paraformaldehyde (4%). Blocking and staining procedure was performed in PBS with 0.3% Triton X-100 (Sigma-Aldrich) and 3% Donkey serum, using the anti-HCN4 antibody (1:200, Alomone Labs). Nuclei were stained with 0,5 μg/mL DAPI. A Video Confocal Microscope (ViCo, Nikon) was used to acquire images. Corrected total cell fluorescence (CTCF) was analyzed by ImageJ software as Integrated density (area of ROI X mean fluorescence of background). Four different ROI and background readings were analyzed for each image and data averaged.

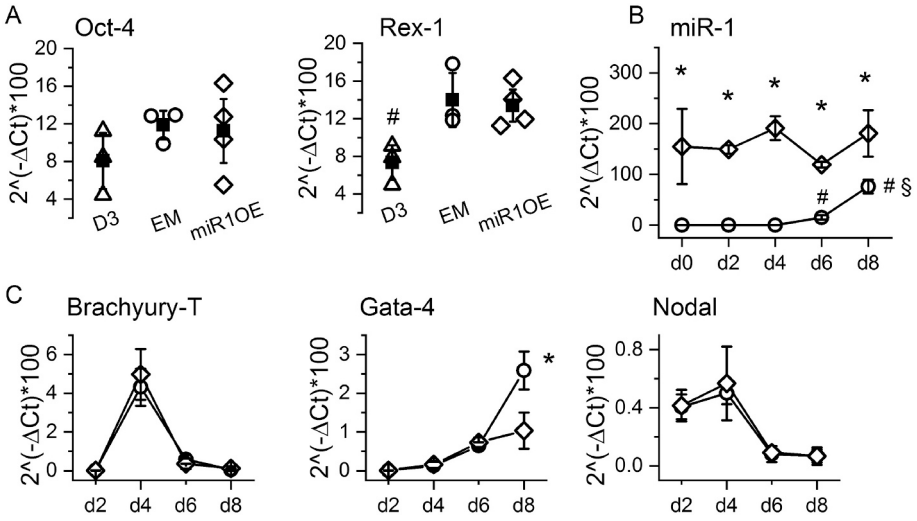

Fig. 1. miR-1 overexpression in mES neither alters pluripotency nor differentiation capacity.
(A) qRT-PCR analysis of the pluripotency genes Oct-4 and Rex-1 in the mES parental line D3 (triangles) and in the engineered mES lines EM (circles) and miR1OE (diamonds). Mean ± SEM values are reported overlapped as filled squares. GAPDH has been used as reference gene. (B) qRT-PCR analysis of miR-1 expression in the engineered miR1OE (diamonds) and EM (circles) mESC lines, from d0 to d8 of differentiation; miR-16 has been used as housekeeping miRNA. (C) qRT-PCR analysis of three early germ layer markers in mES lines EM (circles) and miR1OE (diamonds), from d0 to d8 of differentiation. Brachyury-T for early mesoderm, GATA-4 for early endoderm and Nodal for early ectoderm. GAPDH has been used as reference gene. *Indicates $p < 0.05$ by Student's *t*-test; #Indicates $p < 0.05$ by One-Way Anova vs d0,2,4; §$p < 0.05$ vs day6.

2.6. Neonatal rat ventricular cardiomyocytes (NRVC) transfection

All animal procedures were in accordance with the Italian and UE laws (D. Lgs n° 2014/26, 2010/63/UE) and approved by the committee of the Università degli Studi di Milano and by the Italian Minister of Health (protocol number 1197/2015).

NRVC were isolated from 3 days-old rat pups (Sprague Dawley, Envigo S.R.L.) as previously described [14]. Cardiomyocytes plated on 35 mm dishes were transiently transfected with the same pEZX-MR04 and empty plasmid CmiR0001-MR04, one day after isolation by Lipofectamine 2000 (Life Technologies) following manufacturer's instruction.

2.7. Electrophysiological analysis

Patch-clamp experiments in the whole-cell configuration were carried out on isolated SAN-like cells at day14 seeded on fibronectin (5 μg/cm^2) and on eGFP-NRVCs 30–36 h after transfection. Cells were superfused with Tyrode solution containing (mmol/L): 140 NaCl, 5.4 KCl, 1.8 $CaCl_2$, 1 $MgCl_2$, 10 D-glucose, 5 Hepes-NaOH; pH 7.4. Patch-clamp pipettes had a resistance of 5–7 MΩ when filled with the intracellular-like solution containing (mmol/L): 130 KCl, 10 NaCl, 1 EGTA-KOH, 0.5 $MgCl_2$, 2 ATP (Na-salt), 5 creatine phosphate, 0.1 GTP, 5 Hepes-KOH; pH 7.2. Tyrode was supplemented with 1 mM $BaCl_2$ and 2 mM $MnCl_2$ in order to dissect the funny current (I_f). I_f was activated from a holding potential (hp) of −30 mV applying 10 mV hyperpolarizing voltage steps to the range −35/−125 mV long enough to reach steady-state activation, followed by a fully activating step at −125 mV. Current density was obtained by normalizing current intensity to the cell capacitance. Activation curves were obtained from normalized tail currents at −125 mV and fitted to the Boltzmann equation to obtain the potential at which half of the channels are open ($V_{1/2}$) and the inverse slope factor s. The time constant of activation (τ) have been obtained by fitting the first part of the current traces to a mono-exponential function. Action potentials were recorded in the current-clamp mode from either SAN-like layers or from small spontaneously beating clusters of transfected NRVC (3–5 cells); AP parameters were analyzed as previously reported [15]. In SAN-like cells, conductance was obtained from the linear fit of the I-V data points where current was ohmic; for NRVC conductance was calculated as I/(E-Erev) with E −125 mV and Erev −15 mV. Response of I_f to adrenergic stimulation was evaluated as the shift in the $V_{1/2}$ after superfusing cells with 1 μM isoproterenol dissolved in the extracellular solution. All measures were performed at 36 ± 1 °C.

2.8. Statistical analysis

Statistical analysis was carried out using Origin Pro 9. Groups were compared using One-way ANOVA followed by pairwise comparison using Fisher's test. Student's *t*-test was used to compare two independent populations. For data not normally distributed, we performed a Kolmogorov's Test to compare the population distribution. $P < 0.05$ defines statistical significance. Data are presented as mean ± SEM or median. N indicates the number of experiments, n indicates the number of cells analyzed.

3. Results

3.1. Engineered mESC lines maintain pluripotency and cardiac differentiation potential.

In order to study the effects of miR-1 overexpression on pacemaker cells, we decided to generate stable lines of mESC (D3) expressing miR-1 and EGFP (miR1OE) under the control of a strong constitutive promoter (CMV) or the corresponding empty vector (EM) expressing EGFP only. Plasmids integration was favored by stringent puromycin selection (1 μg/mL) for two weeks. After this, we further selected EGFP-positive cells using a cells sorter (Supplementary Fig. S1).

We first evaluated whether the overexpression of miR-1 and/or EGFP could alter the pluripotency of the engineered cell lines. In Fig. 1A, we reported the expression levels of the pluripotency genes Oct4 and Rex1. Pluripotency markers were equally expressed in miR1OE and EM lines and both lines displayed a significant similar up-regulation of Rex1 compared to the parental D3 line.

We then checked the differentiation potential of these lines through embryoid bodies (EBs) formation. During differentiation from d0 to d8, we analyzed the expression of miR-1 and of Brachyury-T, Gata-4 and Nodal genes, markers of early mesoderm, endoderm and ectoderm, respectively [16]. Fig. 1B, shows the time-course of miR-1 expression in the EBs generated from both engineered lines. As expected, miR-1 is almost not expressed at early days (d0 to d4) in EM EBs and its level increases significantly between d6 and d8. miR-1 levels are constantly high in miR1OE EBs, as expected following overexpression induced by the CMV promoter. Nevertheless, miR1OE line differentiate properly and indeed the early markers of mesoderm, endoderm and ectoderm showed similar time-courses with the exception of GATA4 at d8, whose level was significantly lower in miR1OE than in EM, according to a possible role of miR-1 in the inhibition of endoderm [2].

In order to evaluate the cardiac differentiation potential of the engineered mESC lines, we monitored the percentage of EBs showing

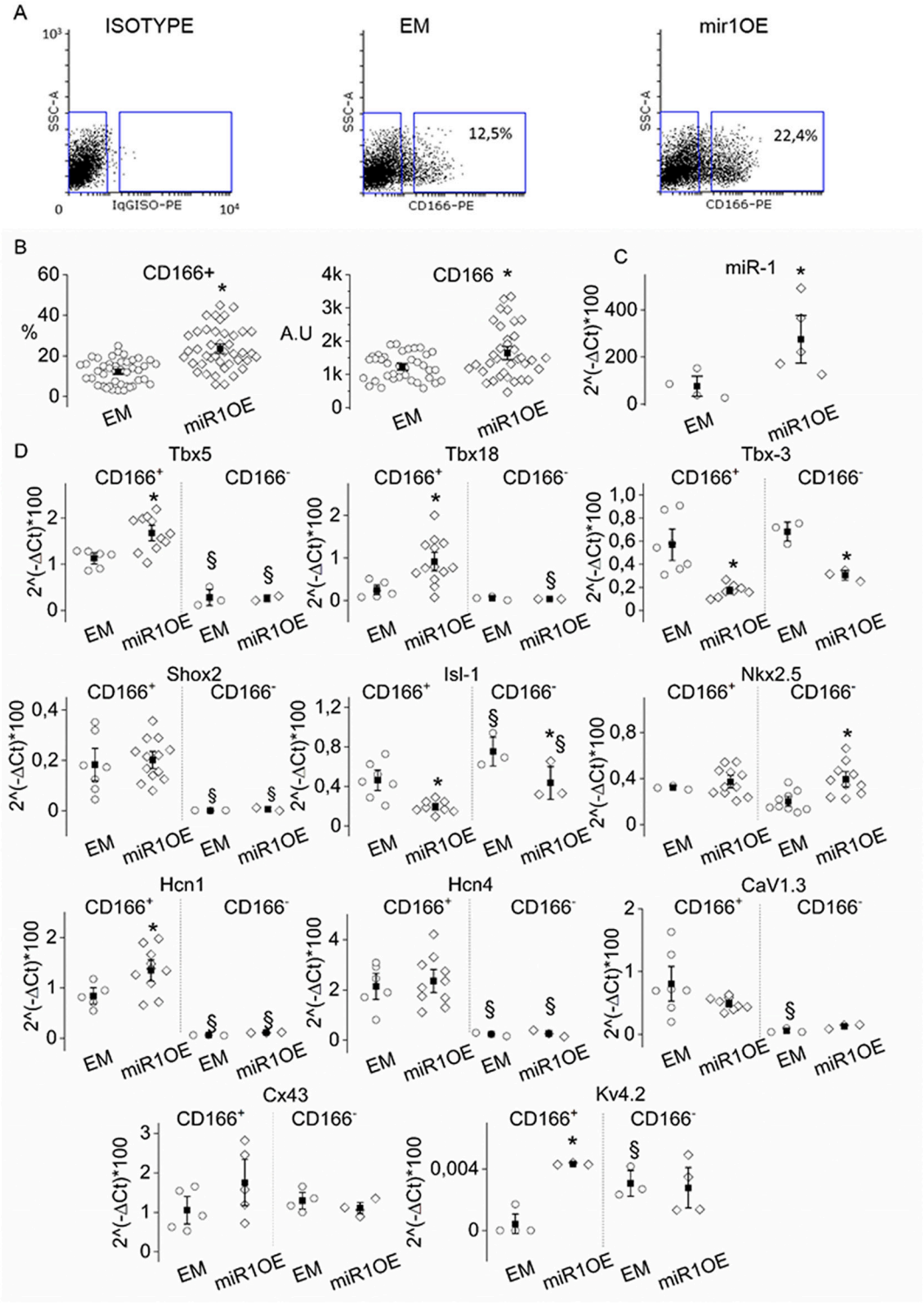

Fig. 2. The miR1OE line generates more CD166$^+$ SAN-like precursors and express higher levels of SAN markers.
(A) Representative dot plots showing the percentage of CD166$^+$ cells at d8 of differentiation in the engineered lines miR1OE and EM; left panel shows the isotype control. (B) left panel: dot plot of the percentage of CD166$^+$ cells at d8 in the engineered miR1OE (diamonds) and EM lines(circles); right panel: plot of the mean fluorescence intensity of CD166 staining in miR1OE (diamonds) and EM (circles) lines. Mean ± SEM values of % and mean fluorescence intensity, reported as filled squares, were: EM CD166$^+$ 12.2 ± 0.9% and 1230.8 ± 65.9 (N = 43); miR-1-OE CD166$^+$ 23.5 ± 1.6% and 1643.4 ± 132 (N = 42). (C) qRT-PCR expression levels of miR-1 in sorted CD166$^+$ cells at d8. (D) qRT-PCR analysis of transcription factors (Tbx3, Tbx5, Tbx18, Shox2, Isl1, Nx2.5), calcium channel Cav1.3 and HCN channel isoforms, connexin 43 and potassium channel Kv4.2 in miR1OE and EM CD166 positive and negative populations at d8. Mean values are reported as filled squares. miR-16 and GAPDH have been used as endogenous reference. *Indicates $p < 0.05$ by Student's *t*-test between miR1OE and EM, while §Indicates $p < 0.05$ by Student's *t*-test between positive and negative populations.

spontaneous contractions. EBs of both lines started to show beating foci around d6–7 and the proportion of beating EBs at d8, was equal: 85.2 ± 5.4% (EM, n = 334, N = 8), 87.6 ± 3.2% (miR1OE, n = 298, N = 8).

In parallel, we generated a mESC line constitutively expressing a siRNA specifically silencing miR-1 and the mCherry reporter (ANTI-miR1). The ANTI-miR1 line expressed the pluripotency markers Oct-4 and Rex-1 at levels comparable with EM and miR1OE lines (supplementary Fig. S2). ANTI-miR1 EBs at d8 showed absence of miR-1 expression (supplementary Fig. S2) and did not display any spontaneous beating, in agreement with the important role of miR-1 in cardiac differentiation/development.

3.2. *miR-1 overexpression increases CD166$^+$ pacemaker precursors and pacemaker transcription factors.*

To specifically isolate and study SAN development, we selected at d8 cells positive for CD166, a marker known to recognize specifically SAN precursors between d6 and d10 of EBs differentiation [12]. FACS analysis revealed a significantly higher percentage of CD166$^+$ cells in the miR1OE line than in the EM line (Fig. 2A and B left panel). Moreover, the miR1OE CD166$^+$ population had a higher mean fluorescence intensity than the EM CD166$^+$ population (Fig. 2B, right panel), indicating an increased expression of CD166 molecules on the plasma membrane. To evaluate a possible effect of miR-1 on cell proliferation EM and mir1OE cells were stained for Ki67 when miR-1 start to be expressed in EM line (d6); flow cytometry data demonstrated that the two cell lines have a similar proliferative potential (EM: 86.3 ± 1.7%, N = 5; miR-1 OE: 83.2 ± 2.0%, N = 5; Supplementary Fig. S3).

We then characterized sorted CD166$^+$ cells for the expression of miR-1 and of several transcription factors involved either in pacemaker development (Tbx5, Tbx18, Tbx3, Shox2, Isl-1) and function (HCN1, HCN4, Cav1.3) or in working myocardium development (Nkx2.5)and function (Cx43, Kv4.2). MiR1OE CD166$^+$ cells, besides showing a significantly higher levels of miR-1 (Fig. 2C), overexpressed also Tbx5 and Tbx18, while Shox2 did not change compared to EM CD166$^+$ cells (Fig. 2D) No differences in CD166$^-$ cells were observed. Tbx3 and Isl-1, both of which participate to SAN development, resulted significantly decreased both in CD166+ and CD166$^-$ miROE cells, pointing to a direct regulation of these factors by miR-1. Nkx2.5 expression did not vary in CD166$^+$ SAN precursor but was instead increased in miR1OE CD166$^-$ cells, confirming a previously reported role of miR-1 in the early phases of working cardiomyocytes development [2].

We also evaluated the expression levels of HCN1, HCN4 and CaV1.3, functional markers of sinus node and of Cx43 and KV4.2 ventricular genes expressed at low levels in SAN cells. [17]. We found HCN1 upregulated in miR1OE CD166$^+$ cells while HCN4, known to interact with miR-1, and Cav1.3 were not modulated. As expected, these three genes were similarly expressed at low levels in CD166$^-$ miR1OE and EM cells (Fig. 2D). We specifically evaluated HCN1 and HCN4 expression also at the protein level; the WB analysis shown in supplementary Fig. S3 clearly demonstrates a significant downregulation only of HCN4 in miR1OE CD166$^+$ cells at d8. Cx43 was not altered neither in CD166$^+$ nor in CD166$^-$ miR1OE cells. KV4.2 was upregulated at d8 but not at d14 (Supplementary Fig. S4C) in miR1OE CD166$^+$, in agreement with previous data [12].

These results support the idea that miR-1 is not only involved in the mesoderm and cardiac differentiation but plays a specific role in sinus node formation.

3.3. *miR1OE SAN-like cells are bradycardic and show altered I_f current.*

CD166$^+$ cells were maintained in culture as monolayers, until d14, for allowing proper maturation into fully competent sinoatrial-like (SAN-like) cells [12]. At this time point, miR-1 was still significantly overexpressed in miR1OE cells (Supplementary Fig. S4A). The functional effect of miR-1 was then assessed on SAN-like cells by patch-clamp analysis. miR1OE SAN-like aggregates had a slower spontaneous rate than EM aggregates (Fig. 3A). The slower rate of miR1OE cells derived from a significantly slower diastolic depolarization (DD) without any change in either take-off potential (TOP) or any other action potential parameter (MDP, APA, APD) (Fig. 3B).

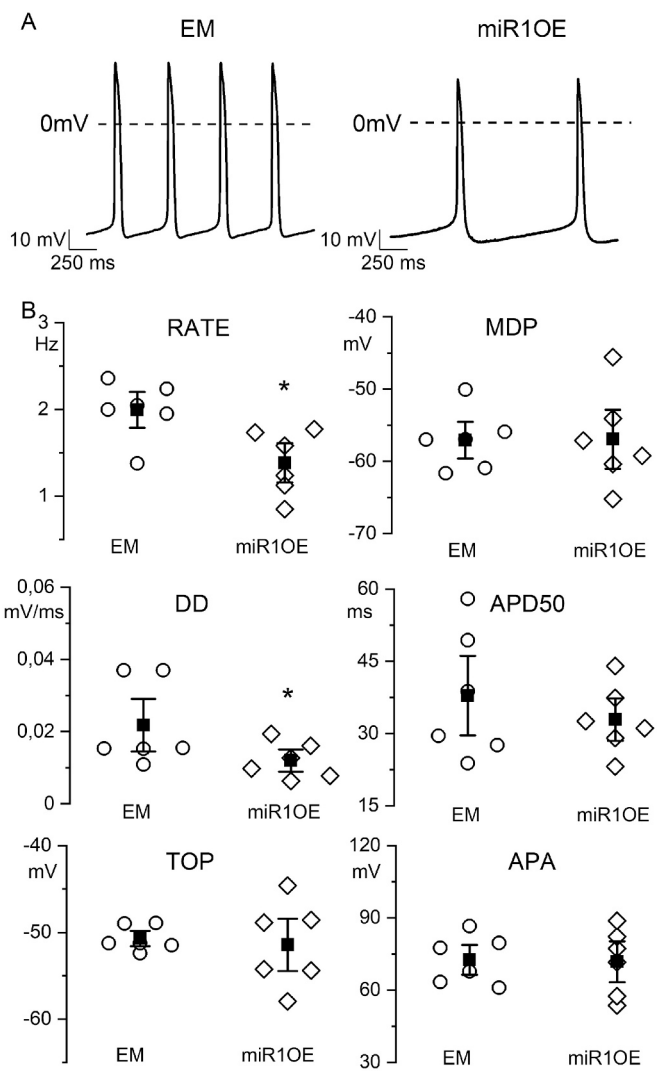

Fig. 3. miR1OE SAN-like cells at d14 shows decreased spontaneous firing rate. (A) Representative spontaneous action potential traces recorded from EM and miR1OE CD166$^+$ clusters, as indicated. (B) Scatter plots of the firing rate, diastolic depolarization (DD) slope, take-off potential (TOP), maximum diastolic potential (MDP), action potential duration at 50% or repolarization (APD50), and action potential amplitude (APA) of miR1OE (diamonds; n = 6, N = 6) and EM SAN-like cells (circles; n = 6, N = 6) at d14. Mean ± SEM values are reported as filled squares. Rate: 1.99 ± 0.14 Hz EM; 1.38 ± 0.15* Hz miR1OE; DD 0.021 ± 0.004 mV/ms EM; 0.012 ± 0.001* mV/ms miR1OE; TOP -51.1 ± 0.5 mV EM; −52.1 ± 1.5 mV miR1OE; APA 72.6 ± 4.1 mV EM, 71.8 ± 5.6 mV miR1OE; APD50: 37.8 ± 5.5 ms EM, 32.9 ± 2.9 ms miR1OE; MDP: −57.1 ± 1.7 mV EM, −56.9 ± 2.7 mV miR1OE. *Indicates $p < 0.05$ by Student's *t*-test.

As previously shown in mouse SAN cells [18] and in mES cell-derived pacemaker cells [13], we found two distinct populations of EM SAN-like cells: one with a fast activating I_f current (time constant $\tau < 1.5$ s at −75 mV) and one with a slow activating I_f ($\tau > 1.5$ s at −75 mV). Left and center panels of Fig. 4A show representative traces while Fig. 4BB depicts the τ plot of fast (empty symbols) and slow (filled symbols) I_f currents. This distinction may derive from the relative contributions of the fast HCN1 and slow HCN4 isoform to I_f, as previously reported [19].

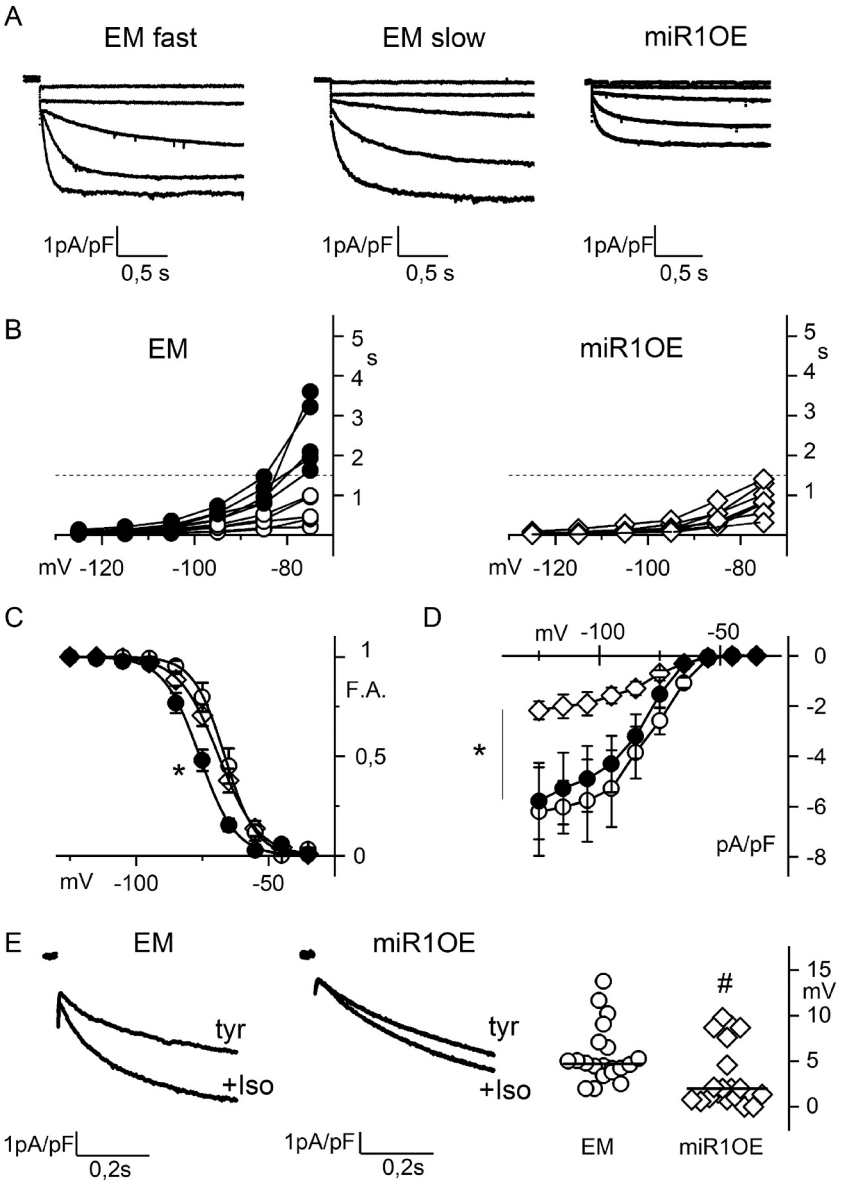

Fig. 4. miR1OE SAN-like cells at d14 display reduced I_f conductance and faster activation kinetics.
(A) Representative traces of I_f current recorded at −35, −55, −75, 95 and −115 mV in EM with fast and slow activation kinetics and in miR1OE SAN-like cells at d14, as indicated. (B) Plots of the activation time constant (τ) of I_f current recorded in EM (circle, left) and in miR1OE (diamonds, right) SAN-like cells. Time constants were arbitrary subdivided into slow (τ > 1.5 s at −75 mV, filled symbol) and fast (τ < 1.5 s at −75 mV, empty symbols). τ mean values were: 2.5 ± 0.3 s EM (n = 6, N = 4) for slow τ; 0.56 ± 0.13 s EM (n = 6, N = 3) and 0.82 ± 0.1 s miR1OE (n = 11, N = 6) for fast τ. (C) Mean activation curves of fast- and slow-activating I_f current in miR1OE and EM SAN-like cells. (Symbols as in B). $V_{1/2}$ and slope values were: −76.2 ± 1.4* mV and 6.5 ± 0.4* mV in EM slow (n = 6, N = 4), −66.7 ± 2.2 mV and 5.2 ± 0.2 mV EM fast (n = 6, N = 3), −68.8 ± 1.7 mV and 6.8 ± 0.7 mV in miR1OE (n = 11, N = 6). (D) Plot of mean I_f current density-voltage relation obtained from miR1OE (diamonds) and EM SAN-like cells (circles). Mean conductance value were: 52.5 ± 13.8 pS/pF (n = 6, N = 4) and 56.4 ± 15.0 pS/pF (n = 6, N = 3) for slow and fast EM, respectively, and 20.2 ± 4.3* pS/pF for fast miR1OE (n = 11, N = 6). (E) left panels: Representative traces of I_f current recorded before (Tyr) and during superfusion of 1 μM isoproterenol (+Iso) at -85 mV in EM and at -75 mV in miR1OE SAN-like cells at d14, as indicated. Right panel: dot plot of the shifts of the I_f activation curve caused by isoproterenol stimulation in EM and miR1OE SAN-like cells. Median is reported as solid line. Median values were:1.75# (n = 20, N = 2) in miR1OE and 4.71 (n = 20, N = 4) in EM SAN-like cells. *Indicates $p < 0.05$ by One-way Anova; #Indicates $p < 0.05$ by Kolmogorov test.

A larger contribution of the positive-activating HCN1 subunit to fast I_f emerged also from the analysis of the mean activation curves; indeed, I_f with fast τ activated at more positive voltages than I_f with slow τ (circles in Fig. 4C). Interestingly, miR1OE SAN-like cells displayed only the fast activating I_f (Fig. 4A and B right panel) which activated at potentials compatible with the fast I_f of EM cells (diamonds in Fig. 4C). Moreover, in accordance with the slower rate, I_f current density was significantly reduced in miR1OE than in EM SAN-like cells (Fig. 4D). No difference in cell capacitance was observed (miR1OE = 32.8 ± 4.7 pF, n = 11, N = 6; EM = 33.9 ± 3.5 pF, n = 12, N = 7).

Since HCN4 is much more responsive to cAMP than HCN1 [20], a specific downregulation of HCN4 is expected to decrease the ability of an adrenergic stimulus to shift I_f activation curve. We challenged EM and miR1OE SAN-like cells with 1 μM isoproterenol and analyzed the shift in I_f $V_{1/2}$. As shown in the representative traces and in the dot plot in Fig. 4E, isoproterenol induced a significantly smaller shift of I_f activation curve in miR1OE cells, a result compatible with a lower contribution of HCN4 to the native current. In Fig. 5A, representative confocal images of SAN-like aggregates at d14, stained with anti-HCN4 antibodies (red) are reported. In agreement with electrophysiological data and with WB analysis at d8, corrected total cell fluorescence analysis highlighted a significantly lower expression of HCN4 in miR1OE than in EM aggregates. Despite this difference, no change in the mRNA levels of HCN channels was observed at d14 (Supplementary Fig. S4C).

The presence of only the fast-activating I_f and the decrease of I_f density, together with the down-regulation of HCN4 staining, demonstrate a specific role of miR-1 in the translational repression of the HCN4 isoform.

3.4. *Neonatal rat ventricular cardiomyocytes transfected with miR-1show reduced beating rate and I_f current density.*

To prove that the functional alterations on the beating rate and the I_f current in SAN-like cells were not caused by the developmental effect of miR-1 on SAN precursors, we transiently transfected, with the same plasmids used to generate engineered mES lines, neonatal rat ventricular cardiomyocytes (NRVC) and carried out electrophysiological experiments on EGFP positive NRVC after 48 h. We chose NRVC because they are spontaneously active and express an I_f current carried mainly by HCN4 and HCN2 [21,22]. The spontaneous beating rate of EM NRVCs showed a large variability, with rates ranging from 0.52 to 4.74 Hz. NRVC overexpressing miR-1 instead displayed a lower variability and

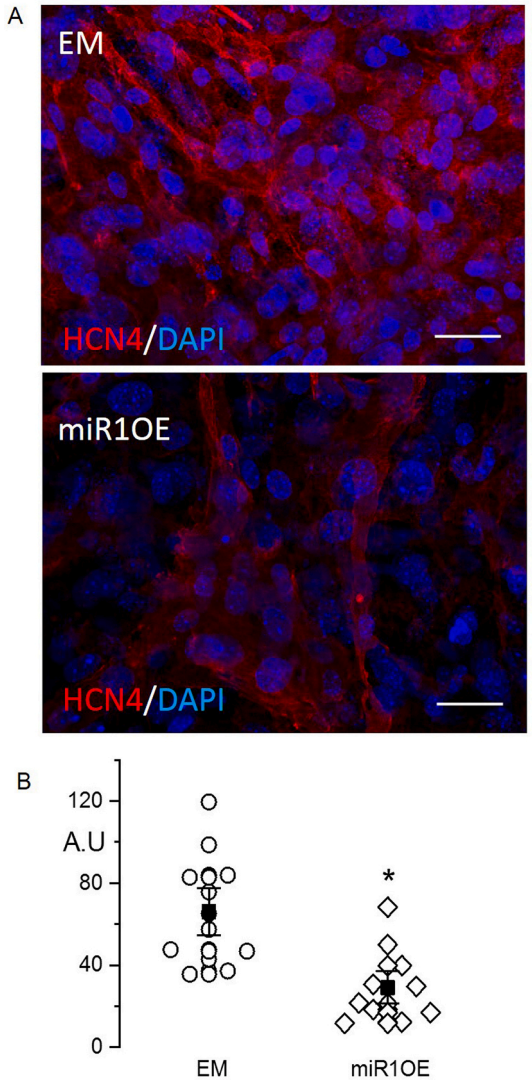

Fig. 5. miR-1 overexpression decreases HCN4 staining in SAN-like cells. (A) Representative images of EM and miR1OE SAN-like cells stained with anti-HCN4 antibodies. Nuclei were counterstained with DAPI. Scale bar: 20 μm. (B) Scatter plot of the corrected total cell fluorescence (CTCF) of HCN4 staining analyzed on EM and miR1OE SAN-like cells. Mean ± SEM values, reported as filled squares, were: 66102.2 ± 7637 in EM (n = 12, N = 2); 29,124.5 ± 5273* in miR1OE (n = 11, N = 2). *Indicates $p < 0.05$ by Student's *t*-test.

significantly lower rates ($p < 0.05$ by Kolmogorov's test, Fig. 6A).

As in SAN-like cells, we found that miR1-NRVC showed a significantly smaller I_f current than EM-NRVC, as highlighted by the mean conductance analysis (Fig. 6B left); no change in the activation curves was found (Fig. 6B right).

In conclusion, we have demonstrated that miR-1 exerts a dual epigenetic modulation on SAN-like cells: during the development, regulating the quote of sinus node precursors and in the mature SAN, modulating the I_f current and consequently the beating rate.

4. Discussion.

MicroRNAs are now recognized as important epigenetic modulators of cardiac pathophysiology. Among the thousands of miRNAs discovered so far, miR-1 is the most abundant in the heart and alterations in its level contribute to heart remodeling both during embryonic development and under specific physiological and pathological conditions [7].

Previous *in vivo* developmental studies analyzed the effect of miR-1 overexpression under the control of the β-myosin heavy chain promoter and revealed a decrease in the proliferation of ventricular myocytes, through the inhibition of Hand2 [5]. Overexpression of miR-1 under the control of α-myosin heavy chain promoter caused hypoplasia of the cardiac ventricular conduction system [6], and atrioventricular block in rodents [23], which appeared to dependent upon repression of the potassium channel Kir2.1 and the gap junction protein connexin 43 [8]. Besides these pieces of evidence, a direct role of miR-1 on sinus node development has not been reported yet.

Here we generated a mESC line constitutively overexpressing miR-1 and the relative control line and used a previously published method for isolating a pure population of $CD166^+$ SAN precursors from differentiating mESC, which mature in culture into fully functional SAN-like cells [12].

Importantly, the overexpression of miR-1, whose expression is normally negligible in undifferentiated mESC, did not impair either pluripotency or differentiation potency and indeed all three germ layers can be promptly generated upon EB formation. The only difference found was an inhibition of the early endoderm marker GATA-4 at d8, in agreement with previously reported data [2]. On the contrary, we demonstrated that, upon differentiation, miR-1 not only generated a percentage of CD166+ SAN-like cells twice that of control mES, but the level of CD166 was also higher. Interestingly, the data showing that, at d8, miR-1 expression in EM EBs is around half that in miR1OE EBs, together with the evidence that ANTI-miR1 EBs do not display any spontaneous beating, point out to a dose-dependent effect of miR-1. Moreover, the evidence that the early cardiac marker Brachyury have an identical time course of expression in EM and miR1OE lines rules out the possibility that the increased proportion of SAN precursors derives from a miR-1-dependent acceleration of development.

It is known that SAN progenitors develop around E8.5 from the sinus horns cells that express Tbx5 and Tbx18 while are negative for Nkx2.5, an inhibitor of the pacemaker gene program [17,24]. Interestingly, at d8, miR1OE $CD166^+$ cells showed significantly higher expression levels of both Tbx5 and Tbx18 while at the same time Nkx2.5 expression remained low. It is noteworthy that Nkx2.5 resulted instead upregulated in the miR81OE CD166-negative population compared to EM CD166-negative cells, in accordance with the role of miR-1 in the early development of $Nkx2.5^+$ cardiac chamber precursors [2].

Tbx3 plays an important role in the maintenance of SAN identity, by downregulating atrial gene program, rather than in promoting directly SAN development as evidenced by the fact that the HCN4+ SAN primordia develop also in the absence of Tbx3 [25]. The decrease of Tbx3 expression in miR1OE cells is not surprising; indeed, it was seen to be downregulated together with HCN4 in trained animals [11] and moreover bioinformatics data identify Tbx3 as a target of miR-1 (miRDB.org). The decrease in Isl-1 expression is less clear; however, at early phases (E8), SAN progenitors develop from Isl-1 negative cells that only later start to express Isl-1 [17].

Beyond its role in cardiac development, miR-1 is modulated by various pathological and physiological stimuli (*e.g.* hypertrophy, atrial fibrillation and endurance training) causing, among other effects, alteration in the normal heart rhythm. In both animal models and humans, for example, intense aerobic training causes mild ventricular hypertrophy and bradycardia. These latter physiological changes are accompanied by a decrease of miR-1 in the ventricle [26] and an increase in the SAN [11]. In these scenarios, changes in miR-1 have been associated with alteration in the pacemaker HCN channels, but no direct effects have been demonstrated. It is interesting to report that in mouse SAN the expression level of miR-1 is lower compared to that in ventricles (Supplementary Fig. S4B) and thus miR-1 levels result inversely proportional to I_f current density in these regions of the hearts. On this regard, Luo and colleagues demonstrated that down regulation of miR-1/miR-133 contributes to re-expression of pacemaker channel genes HCN2 and HCN4 in hypertrophic hearts [27]. miR-1 was found downregulated also in atria and ventricles affected by cardiac arrhythmias

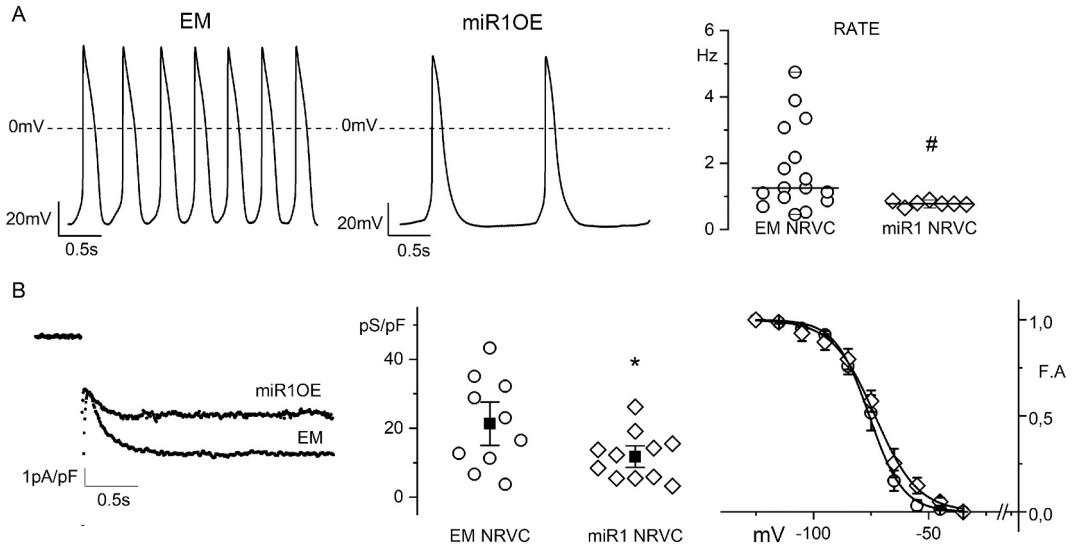

Fig. 6. NRVCs over expressing miR-1 show both decreased spontaneous firing rate and I_f conductance.
(A) Representative spontaneous action potential traces recorded from EM and miR1OE NRVCs, as indicated. Right panel, scatter plot of action potential rate of spontaneously beating NRVCs transfected with the empty (circles; n = 16, N = 5) or miR-1 vectors (diamonds; n = 7, N = 5). Median is shown as a solid line. Parameters values were: median rate 1.25 Hz EM; 0.78 Hz miR1OE. (B) Left, representative current traces recorded at −125 mV, from transfected NRVC as indicated; center, dots plot of mean I_f current conductance in EM (circles) and miR1OE (diamonds) NRVC. Mean conductance values (filled squares) were: 21.3 ± 4.2 pS/pF EM-NRVC (n = 10, N = 5); 11.8 ± 2.1 pS/pF miR1OE-NRVC (n = 11, N = 5). Right, mean activation curves of I_f current from miR1OE and EM-NRVC (symbols as in top panel). Mean $V_{1/2}$ and inverse slope factor values were: −76 ± 2.1 mV and 5.2 ± 0.7 mV EM (n = 11, N = 5), −74 ± 2.5 mV and 8.6 ± 1.1 mV miR1OE (n = 7, N = 5). *Indicates $p < 0.05$ by Student's *t*-test; #Indicates $p < 0.05$ by Kolmogorov's test.

such as atrial fibrillation or ventricular tachyarrhythmia, while the expression of several ion channels, among which HCN2, HCN4 was found upregulated [8,28,29]. On the contrary, up-regulation of miR-1 level in SAN can affect heart automaticity; D'Souza and coworkers demonstrated that in sinus node of trained animal models (mice and rats), which displayed intrinsic bradycardia and a decreased I_f current, miR-1 was upregulated [11]. Nevertheless, whether the decreased I_f was a direct consequence of miR-1 dysregulation was not assessed.

In the present work we provided a direct evidence that miR-1 upregulation causes a decrease in SAN-like cells rate due to I_f modulation. The lack of differences in qRT-PCR data together WB and immunofluorescence data showing a specific downregulation of HCN4 protein demonstrate that miR-1 modulate HCN4 by inhibiting mRNA translation rather than mRNA stability. This decrease translates into a significant decrease in the firing rate and in the I_f current density both in miR1OE SAN-like cells and in NRVC transiently overexpressing miR-1. This last evidence ruled out the possibility that the differences observed were the consequence of an inappropriate SAN development under constantly high levels of miR-1, but it was rather a direct epigenetic modulation of the pacemaker I_f current. Our data showing that in EM cells miR-1 expression rise from d4 to d8 and then falls again at d14 is in agreement with the previously shown raise in rate of SAN-like cells during prolonged culture, which recapitulate the physiological increase in heart rate observed during mouse embryonic and postnatal development [12].

It is known that miRNA may act either by degrading the target mRNA or by preventing its translation [30]. Because bioinformatic data (*e.g.* miRTareBase) show that HCN4 and HCN2, but not HCN1, displays a miR-1 consensus sequence, we evaluated the expression of HCN1, 2 and 4 isoforms in control and miR1OE $CD166^+$ cells. HCN1 was slightly but significantly upregulated at early stage of differentiation (d8) a difference that disappeared at d14, when functional analysis was carried out. In agreement with previous data and with its role in the working myocardium [12], HCN2 expression was negligible in SAN-like cells, independently of the miR-1 levels. HCN4 transcript, the main isoform of the sinoatrial I_f current [12], was unaltered by miR-1 over-expression both at d8 and d14. These data indicate that miR-1 act as an inhibitor of translation and are in accordance with a previous report showing that HCN4 and HCN2 mRNA levels were unchanged following antagomiR-1 treatment while protein levels of both isoforms were upregulated in the border zone of rat with myocardial infarction [31]. To evaluate an isoform specific functional effect of miR-1, we analyzed the kinetic properties (activation time constants (τ) and $V_{1/2}$) of the I_f current, which strictly depend on HCN isoforms expressed on the plasma membrane. HCN1 channels expressed in HEK cells show indeed faster τ (~0.5 s at −75 mV) and a 6.5 mV positive shift of $V_{1/2}$ than HCN4 channels (τ > 6 s at −75 mV) [19]. In native mouse SAN, and in mES-derived pacemaker cells [13,18], two populations of cells can be identified that express either a fast or slow-activating I_f; which likely derive from a different ratio of HCN4/HCN1 expression. While EM SAN-like cells display, as expected, both fast and slow-activating I_f, the latter activating at more hyperpolarized potentials, we have found here that miR1OE SAN-like cells show only the fast-activating and depolarized I_f. Moreover, we found that miR1OE cells show a decreased responsiveness to isoproterenol than EM cells. Although it is conceivable that the reduction of HCN4 may indirectly impact on the assembly of naïve hetero-tetrameric channels, our results are compatible with miR1OE f-channels having a more prevalent contribution of the fast activating, cAMP-insensitive HCN1 subunit; this is also supported by WB analysis that shows a decreased HCN4 but an unaltered HCN1 expression. A similar change in I_f time constants, but not in the $V_{1/2}$, has been previously reported in SAN cardiomyocytes in which the expression of HCN4 was genetically knocked out in adult mice [32]. Our electrophysiological data, together with immunofluorescence analysis of HCN4 expression in SAN-like aggregates (Fig. 5) clearly demonstrate that miR-1 over-expression specifically and significantly decreases the levels of the slowly activating HCN4 isoform.

It is interesting to report that when $CD166^-$ cells are re-aggregated and plated similarly to $CD166^+$ cells, EM $CD166^-$ cells showed small sparce spontaneously contracting regions, while miR1OE $CD166^-$ cells showed extended spontaneously contracting regions. However, the rate of contraction was similar (EM: 0.6 ± 0.2 Hz; miR1OE: 0.8 ± 0.1 Hz) and significantly lower than that of the $CD166^+$ counterparts (see Fig. 3). The larger beating area of miR1OE $CD166^-$ cells agree with the previously shown role of miR-1 in general cardiac mesoderm commitment

[2].

These findings consolidate the role of miR-1 as a fine modulator of cardiac automaticity. We have previously shown that the beating rate of mES-derived SAN-like cells increases with time in culture from d8 to d25 [12] and here we show by qPCR that in control EM line the levels of endogenous miR-1 decrease between d8 (75.9 ± 28.5) and d14 (26.5 ± 4.9) (see Figs. 2C and S4A). In line with the epigenetic role of miR-1 in controlling cardiomyocytes automaticity, it is noteworthy to mention that neonatal ventricular cardiomyocytes, which spontaneously beat and express HCN2 and HCN4 isoforms [21,22], become quiescent at later stage of maturation due to a reduction in the I_f current [33]. Here we show that indeed mouse heart ventricles express higher levels of miR-1 than SAN and atria (see Supplementary Fig. S4B). It is however important to underline that overexpression of miR-1 in SAN-like cells does not induce a switch in cell fate from SAN to ventricle as confirmed by the fact that ventricular genes (HCN2, CX43 and Kv4.2) are not modulated in $CD116^+$ cells(supplementary Fig. S4C).

The present study unravels for the first time a double role of miR-1 in sinus node; at early stage of cardiac development, increasing levels of miR-1 ensure the proper development of the cardiac mesoderm, in general, and of sinoatrial precursors, in particular. At later stages, once the mature SAN is formed, miR-1 plays a direct role in the functional expression of the HCN4 isoform that contribute to the I_f current and thus to the modulation of heart rate. This epigenetic modulation may be of particular importance for those conditions, such as atrial fibrillation and sick sinus syndrome in which miR-1 levels are modulated, leading to a pathological dysregulation of ion channels and cell excitability [34].

Funding.

This research did not receive any specific grant from funding agencies in the public, commercial, or not-for-profit sectors.

Declaration of Competing Interest.

None.

Acknowledgements

We thank Dr. Mark R. Boyett for kindly providing the pEZX-MR04 plasmid.

Appendix A. Supplementary data.

Supplementary data to this article can be found online at https://doi.org/10.1016/j.yjmcc.2021.05.001.

References

[1] Y. Liang, D. Ridzon, L. Wong, C. Chen, Characterization of microRNA expression profiles in normal human tissues, BMC Genomics 8 (2007) 166.
[2] K.N. Ivey, A. Muth, J. Arnold, F.W. King, R.F. Yeh, J.E. Fish, et al., MicroRNA regulation of cell lineages in mouse and human embryonic stem cells, Cell Stem Cell 2 (2008) 219–229.
[3] Y. Zhao, E. Samal, D. Srivastava, Serum response factor regulates a muscle-specific microRNA that targets Hand2 during cardiogenesis, Nature 436 (2005) 214–220.
[4] K. Wystub, J. Besser, A. Bachmann, T. Boettger, T. Braun, miR-1/133a clusters cooperatively specify the cardiomyogenic lineage by adjustment of myocardin levels during embryonic heart development, PLoS Genet. 9 (2013), e1003793.
[5] T.E. Callis, D.Z. Wang, Taking microRNAs to heart, Trends Mol. Med. 14 (2008) 254–260.
[6] E. Samal, M. Evangelista, G. Galang, D. Srivastava, Y. Zhao, V. Vedantham, Premature microRNA-1 expression causes hypoplasia of the cardiac ventricular conduction system, Front. Physiol. 10 (2019) 235.
[7] D.A. Chistiakov, A.N. Orekhov, Y.V. Bobryshev, Cardiac-specific miRNA in cardiogenesis, heart function, and cardiac pathology (with focus on myocardial infarction), J. Mol. Cell. Cardiol. 94 (2016) 107–121.
[8] G. Santulli, G. Iaccarino, N. De Luca, B. Trimarco, G. Condorelli, Atrial fibrillation and microRNAs, Front. Physiol. 5 (2014) 15.
[9] L. Elia, R. Contu, M. Quintavalle, F. Varrone, C. Chimenti, M.A. Russo, et al., Reciprocal regulation of microRNA-1 and insulin-like growth factor-1 signal transduction cascade in cardiac and skeletal muscle in physiological and pathological conditions, Circulation 120 (2009) 2377–2385.
[10] S. Gielen, G. Schuler, V. Adams, Cardiovascular effects of exercise training: molecular mechanisms, Circulation 122 (2010) 1221–1238.
[11] A. D'Souza, A. Bucchi, A.B. Johnsen, S.J. Logantha, O. Monfredi, J. Yanni, et al., Exercise training reduces resting heart rate via downregulation of the funny channel HCN4, Nat. Commun. 5 (2014) 3775.
[12] A. Scavone, D. Capilupo, N. Mazzocchi, A. Crespi, S. Zoia, G. Campostrini, et al., Embryonic stem cell-derived CD166+ precursors develop into fully functional sinoatrial-like cells, Circ. Res. 113 (2013) 389–398.
[13] A. Barbuti, A. Crespi, D. Capilupo, D. Mazzocchi, M. Baruscotti, D. Di Francesco, Molecular composition and functional properties of f-channels in murine embryonic stem cell-derived pacemaker cells, J. Mol. Cell. Cardiol. 46 (3) (2009) 343–351.
[14] D. Avitabile, A. Crespi, C. Brioschi, V. Parente, G. Toietta, P. Devanna, et al., Human cord blood CD34+ progenitor cells acquire functional cardiac properties through a cell fusion process, Am. J. Physiol. Heart Circ. Physiol. 300 (2011) H1875–H1884.
[15] A. Bucchi, M. Baruscotti, R.B. Robinson, D. DiFrancesco, Modulation of rate by autonomic agonists in SAN cells involves changes in diastolic depolarization and the pacemaker current, J. Mol. Cell. Cardiol. 43 (2007) 39–48.
[16] A. Leahy, J.W. Xiong, F. Kuhnert, H. Stuhlmann, Use of developmental marker genes to define temporal and spatial patterns of differentiation during embryoid body formation, J. Exp. Zool. 284 (1999) 67–81.
[17] A. Barbuti, R.B. Robinson, Stem cell-derived nodal-like cardiomyocytes as a novel pharmacologic tool: insights from sinoatrial node development and function, Pharmacol. Rev. 67 (2015) 368–388.
[18] M.E. Mangoni, J. Nargeot, Properties of the hyperpolarization-activated current (I (f)) in isolated mouse sino-atrial cells, Cardiovasc. Res. 52 (2001) 51–64.
[19] C. Altomare, B. Terragni, C. Brioschi, R. Milanesi, C. Pagliuca, C. Viscomi, et al., Heteromeric HCN1-HCN4 channels: a comparison with native pacemaker channels from the rabbit sinoatrial node, J. Physiol. 549 (2003) 347–359.
[20] C. Viscomi, C. Altomare, A. Bucchi, E. Camatini, M. Baruscotti, A. Moroni, et al., C terminus-mediated control of voltage and cAMP gating of hyperpolarization-activated cyclic nucleotide-gated channels, J. Biol. Chem. 276 (2001) 29930–29934.
[21] W. Shi, R. Wymore, H. Yu, J. Wu, R.T. Wymore, Z. Pan, et al., Distribution and prevalence of hyperpolarization-activated cation channel (HCN) mRNA expression in cardiac tissues, Circ. Res. 85 (1999) e1–e6.
[22] T. Muto, N. Ueda, T. Opthof, T. Ohkusa, K. Nagata, S. Suzuki, et al., Aldosterone modulates I(f) current through gene expression in cultured neonatal rat ventricular myocytes, Am. J. Physiol. Heart Circ. Physiol. 293 (2007) H2710–H2718.
[23] Y. Zhang, L. Sun, Y. Zhang, H. Liang, X. Li, R. Cai, et al., Overexpression of microRNA-1 causes atrioventricular block in rodents, Int. J. Biol. Sci. 9 (2013) 455–462.
[24] J.H. van Weerd, V.M. Christoffels, The formation and function of the cardiac conduction system, Development 143 (2016) 197–210.
[25] W.M. Hoogaars, A. Engel, J.F. Brons, A.O. Verkerk, F.J. de Lange, L.Y. Wong, et al., Tbx3 controls the sinoatrial node gene program and imposes pacemaker function on the atria, Genes Dev. 21 (2007) 1098–1112.
[26] T. Fernandes, V.G. Barauna, C.E. Negrao, M.I. Phillips, E.M. Oliveira, Aerobic exercise training promotes physiological cardiac remodeling involving a set of microRNAs, Am. J. Physiol. Heart Circ. Physiol. 309 (2015) H543–H552.
[27] X. Luo, H. Lin, Z. Pan, J. Xiao, Y. Zhang, Y. Lu, et al., Down-regulation of miR-1/miR-133 contributes to re-expression of pacemaker channel genes HCN2 and HCN4 in hypertrophic heart, J. Biol. Chem. 283 (2008) 20045–20052.
[28] Z. Girmatsion, P. Biliczki, A. Bonauer, G. Wimmer-Greinecker, M. Scherer, A. Moritz, et al., Changes in microRNA-1 expression and IK1 up-regulation in human atrial fibrillation, Heart Rhythm 6 (2009) 1802–1809.
[29] A. Curcio, D. Torella, C. Iaconetti, E. Pasceri, J. Sabatino, S. Sorrentino, et al., MicroRNA-1 downregulation increases connexin 43 displacement and induces ventricular tachyarrhythmias in rodent hypertrophic hearts, PLoS One 8 (2013), e70158.
[30] B. Yang, Y. Lu, Z. Wang, Control of cardiac excitability by microRNAs, Cardiovasc. Res. 79 (2008) 571–580.
[31] H.D. Yu, S. Xia, C.Q. Zha, S.B. Deng, J.L. Du, Q. She, Spironolactone regulates HCN protein expression through micro-RNA-1 in rats with myocardial infarction, J. Cardiovasc. Pharmacol. 65 (2015) 587–592.
[32] S. Herrmann, J. Stieber, G. Stockl, F. Hofmann, A. Ludwig, HCN4 provides a 'depolarization reserve' and is not required for heart rate acceleration in mice, EMBO J. 26 (2007) 4423–4432.
[33] K. Yasui, W. Liu, T. Opthof, K. Kada, J.K. Lee, K. Kamiya, et al., I(f) current and spontaneous activity in mouse embryonic ventricular myocytes, Circ. Res. 88 (2001) 536–542.
[34] O. Monfredi, M.R. Boyett, Sick sinus syndrome and atrial fibrillation in older persons - a view from the sinoatrial nodal myocyte, J. Mol. Cell. Cardiol. 83 (2015) 88–100.